THE JOURNAL OF PHYSICAL CHEMISTRY Letters

Letter

Cite This: J. Phys. Chem. Lett. 2018, 9, 2985−2990

pubs.acs.org/JPCL

Similarity Between Amorphous and Crystalline Phases: The Case of TiO_2

Juraj Mavračić,[†,‡] Felix C. Mocanu,[‡] Volker L. Deringer,[‡,§] Gábor Csányi,[§] and Stephen R. Elliott*[,‡]

[†]Department of Physics, Cavendish Laboratory, [‡]Department of Chemistry, and [§]Department of Engineering, University of Cambridge, Cambridge CB2 1TN, United Kingdom

Supporting Information

ABSTRACT: Amorphous and crystalline materials differ in their long-range structural order. On the other hand, short-range order in amorphous and crystalline materials often appears similar. Here, we use a recently introduced method for obtaining quantitative measures for structural similarity to compare crystalline and amorphous materials. We compare seven common crystalline polymorphs of TiO_2, all assembled out of TiO_6 or TiO_7 polyhedral building blocks, to liquid and amorphous TiO_2 in a quantitative two-dimensional similarity plot. We find high structural similarity between a model of amorphous TiO_2, obtained by *ab initio* molecular-dynamics, and the B-TiO_2 crystalline polymorph. The general approach presented here sheds new light on a long-standing controversy in the structural theory of amorphous solids.

The major difference between amorphous and crystalline materials lies in the long-range structural order. While an ideal crystal can always be exactly defined via the periodic translation of a single unit cell, the lack of inherent periodicity makes such an approach impossible for the amorphous phase, although there is often an appreciable degree of short-range and even medium-range order. However, the extent of any structural similarity between an amorphous phase and its corresponding crystalline polymorphs has, hitherto, been impossible to quantify. Here, we describe a new approach for obtaining a quantitative measure for the structural similarity between amorphous and crystalline phases, with an application to the case of TiO_2.

Amorphous materials are important in many areas of application, such as optical fibers, displays, solar cells, thermal transport and batteries.[1−6] In some of them, the transition between the amorphous and crystalline phases lies at the heart of operation. Examples include phase-change (PC) memory devices and biodegradable implants.[7,8] While applications of crystalline materials have been studied extensively, the search for useful amorphous counterparts has been relatively sparse. This is partly due to limited experimental characterization of the amorphous structure and the lack of accurate structural models. Progress has been made with the advance of reliable computational techniques, and it is now possible to simulate the amorphous−crystalline phase transition in PC materials at experimental time scales using density functional theory (DFT).[9−11] On the other hand, while structural data on particular amorphous systems is collected, little progress has been made on a fundamental understanding of the structure of the amorphous state itself.

Historically, two different paradigms about the structure of amorphous solids were formulated in the 1950s, namely, the crystallite theory and the random network theory.[12] These two paradigms evolved into a modern structural theory of amorphous solids. Crystallites have been replaced by short-range order, and random, by the absence of long-range order. Thus, the modern interpretation considers structurally similar building blocks connected in a network, where intermediate-range order, that is, order on a scale larger than that of the individual building blocks, might still persist to a certain degree. However, fundamental questions remain. Specifically, what is the extent of intermediate and long-range order in the amorphous structure, i.e., the amount of randomness in the system? Also, how close is the relationship between the fundamental building blocks in amorphous materials and the corresponding crystals?

TiO_2 is an ideal system in which to search for answers to these general questions. It exhibits a variety of crystalline polymorphs, which are all built out of characteristic polyhedral units. Differences between them can be attributed to relative distortions of the units and the varying connectivity between them. In this work, the most accurate structural models of molten and solid a-TiO_2 to date were generated using *ab initio* molecular dynamics (AIMD). These have then been compared to the crystalline structures using the recently developed Smooth Overlap of Atomic Positions (SOAP) method.[13,14]

Snapshots of the generated liquid and amorphous TiO_2 (a-TiO_2) models are shown in Figure 1. Similar to the crystals, the

Received: April 6, 2018
Accepted: May 15, 2018
Published: May 15, 2018

DOI: 10.1021/acs.jpclett.8b01067
J. Phys. Chem. Lett. 2018, 9, 2985−2990

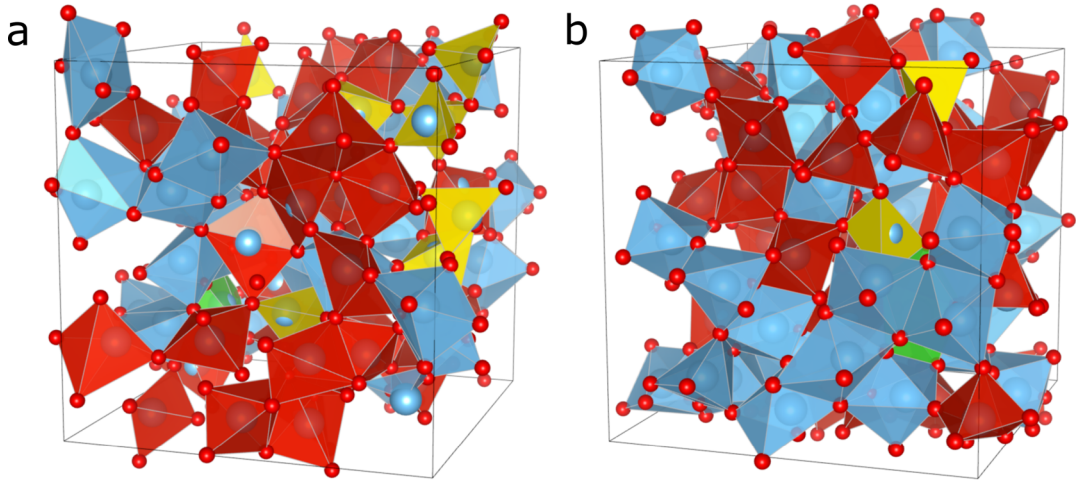

Figure 1. 216-atom models of (a) liquid (2250 K, 3.21 g cm^{-3}) and (b) solid (300 K, 3.57 g cm^{-3}) a-TiO_2, as obtained from AIMD simulations. TiO_4, TiO_5, TiO_6, and TiO_7 polyhedra are shown in yellow, red, blue, and green, respectively.

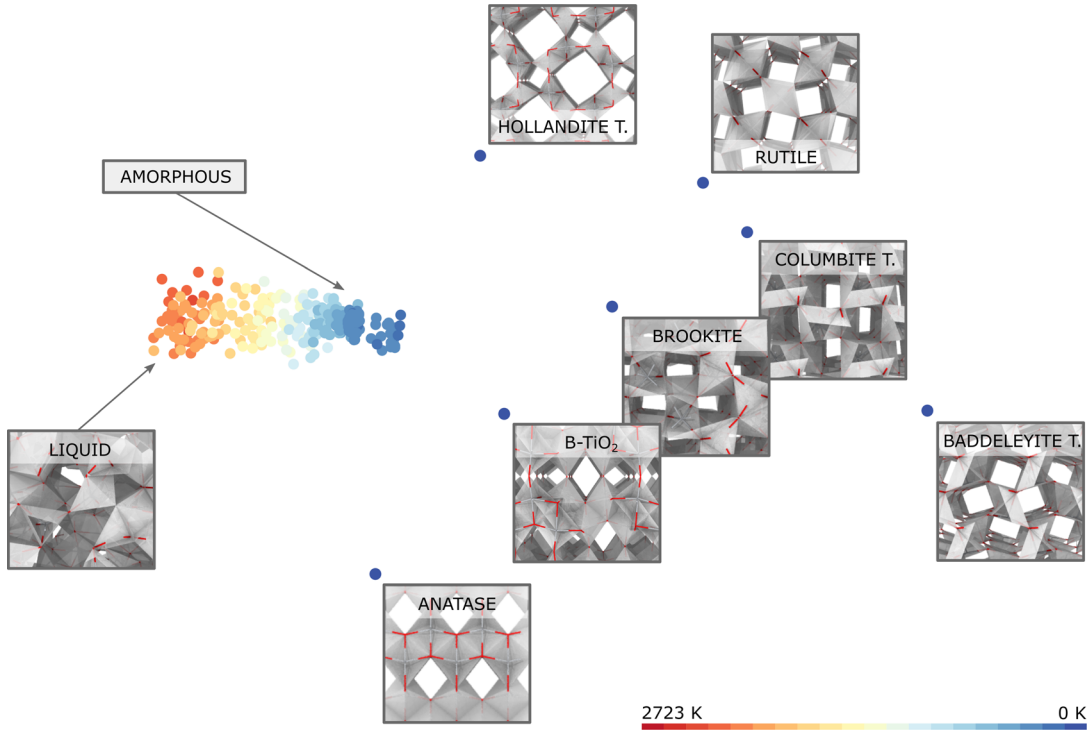

Figure 2. SOAP-based similarity map of configurations of the AIMD TiO_2 model to the corresponding crystalline polymorphs, during quenching from the melt and volume equilibration of the amorphous state. Distances between two structures on the map indicate the degree of structural similarity; the closer, the more similar. The crystal polymorphs investigated are rutile, anatase, brookite, B-TiO_2, baddeleyite-type TiO_2, columbite-type TiO_2, and hollandite-type TiO_2.[19−24] A SOAP cutoff of 4.20 Å was used, and MDS was performed on the SOAP data. Snapshots of relevant structural models are shown. Polyhedral building blocks are shown in gray. Lines indicate bonds around titanium (white) and oxygen (red).

main structural characteristic of both the liquid and amorphous phases are polyhedral units connected via vertices, edges and faces. Visually, little distinction between the liquid and the amorphous solid can be made, except for the different density. However, slight differences appear in the relative amount of different polyhedral units (Supporting Information: Figure S1, Table S1). The proportion of octahedral TiO_6 units is larger in the amorphous phase (49.8%) than in the liquid (29.0%). This trend is in accordance with previous findings, considering the different densities of the phases.[15−17] What about the crystalline polymorphs? Among the crystals studied, all but baddeleyite-type TiO_2 contain TiO_6 building units. This includes the most common crystalline polymorphs of TiO_2, rutile, anatase, and brookite. In baddeleyite-type TiO_2, the units are TiO_7 units. A simple way to quantify the differences between the polymorphs is to count the edges shared between the polyhedral units. Neighboring octahedra share two, three, and four common edges in rutile, brookite, and anatase, respectively. However, the number of common edges can be a direct reflection of the change of the average coordination number. Thus, the ratio of vertex to edge sharing is a more significant indicator for polyhedral connectivity. The vertex/edge-sharing ratio is 4, 2, and 1 for rutile, brookite, and anatase, respectively, and 3.0 for the liquid model and 2.1 for the amorphous model. The value

DOI: 10.1021/acs.jpclett.8b01067
J. Phys. Chem. Lett. 2018, 9, 2985−2990

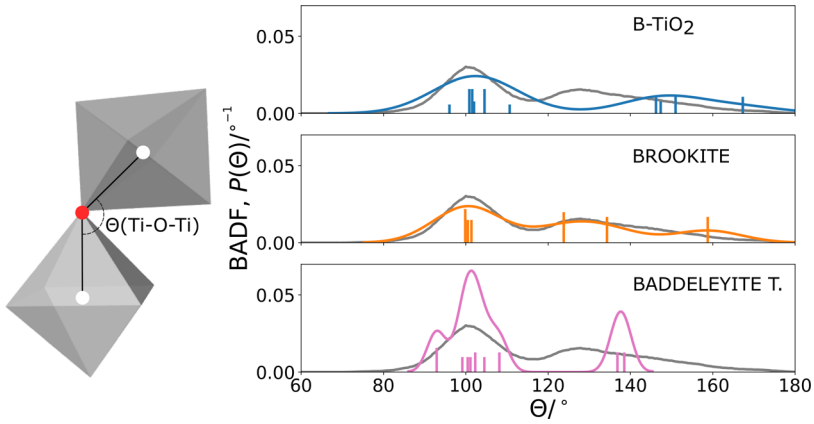

Figure 3. Ti−O−Ti bond-angles and their frequencies (scaled by a factor of 0.1) for some crystalline polymorphs of TiO_2 (vertical lines) compared to the bond-angle distribution function (BADF) of the amorphous structure (gray curve). Only atoms within a 2.75 Å bonding cutoff distance were considered. The colored lines are Gaussian kernel-density estimates[26,27] of the distribution of Ti−O−Ti bond-angles for the corresponding crystalline polymorphs.

for a-TiO_2 is in accordance with previous findings.[18] Perhaps, this indicates a structural similarity between a-TiO_2 and brookite. However, such an analysis is limited, since only one aspect of the structure is considered, namely, polyhedral connectivity. Other aspects, such as the density, the average Ti−O distance, the relative orientation of polyhedral units or the distortion of polyhedral units, are neglected. A more sophisticated structural comparison performed with the SOAP descriptor is presented in Figure 2, where the transition from liquid to amorphous TiO_2 is shown.

The SOAP descriptor takes all structural aspects of the phases into account, providing a distance measure for similarity between each of the phases investigated, yielding an $N \times N$ matrix, where N is the number of structures investigated. To visualize these data in two-dimensional space, multidimensional scaling (MDS), a nonlinear dimensionality-reduction technique, was performed.[25] In this way, relative descriptor-distances are maintained, and an accurate two-dimensional representation of the many-dimensional data is obtained. Thus, distances between points in Figure 2 quantify the similarity between the various structures.

Figure 2 shows that there is more to the structural similarity between phases of TiO_2 than simply polyhedral connectivity. Although the similarity of the amorphous phase at 300 K to brookite is indeed high, the structural similarity to B-TiO_2 is even higher. This is revealed by the shorter distance between B-TiO_2 and amorphous configurations in Figure 2. Another important feature of the similarity map is that a distinction between liquid and solid phases is clearly visible, an indication of their fundamental structural differences. Consistently, the method captures features of increased disorder in the liquid and a narrowing of the distribution for the amorphous phase is observed with decreasing temperature. Nevertheless, structural-similarity results obtained with SOAP can be difficult to interpret intuitively. The vertex/edge sharing ratio between polyhedral units explains the similarity of the amorphous phase to brookite, but no analogous simple argument can be made for the similarity to B-TiO_2. Bond-angle distribution functions (BADFs), on the other hand, provide some insight. The prominent Ti−O−Ti angles for B-TiO_2 and brookite, as well as their relative frequencies, agree to some extent with the BADFs of amorphous TiO_2, whereas there is less agreement between baddeleyite-type TiO_2 and the amorphous phase (Figure 3). A comparison of any single physical quantity, such as the polyhedral connectivity, the BADF or the bond-length, can provide qualitative insight into the similarity, whereas SOAP provides a quantitative measure.

It is expected that a resemblance between amorphous and crystalline short-range order arises as a consequence of local bonding.[12] Ti−O bonding within individual polyhedral units is expected to be similar for all phases. Indeed, a consistent trend between the covalent bond-strength and the Ti−O bond length is observed (Figure 4). The gray line in Figure 4 is a theoretical

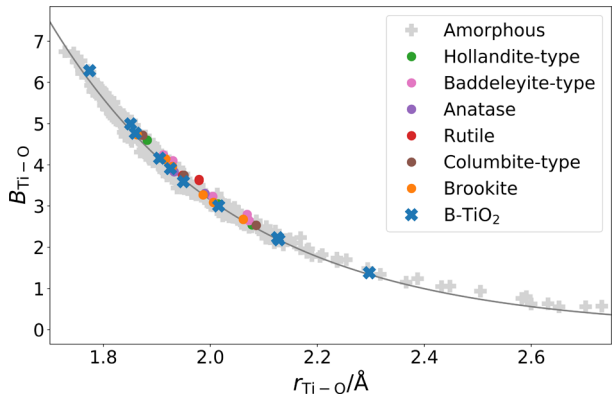

Figure 4. Relationship between Ti−O bond-strengths and Ti−O bond-lengths in crystalline TiO_2 polymorphs (colored symbols) and the amorphous solid (gray symbols). The curve is a fit to the amorphous data, according to the Pauling expression, eq 1.[28]

fit to the amorphous data analogous to the well-known bond-order versus bond-length relationship established by Pauling:[28]

$$B(r_{Ti-O}) = 10^{R_{cov} - r_{Ti-O}/D} \quad (1)$$

Here, $B(r_{Ti-O})$ is the dimensionless bond-strength, calculated as the integral of the projected crystal orbital Hamilton population for a given bond,[29,30] and r_{Ti-O} is the bonding distance. Both D and R_{cov} are constants, and were determined from the fit. While D has no simple physical interpretation, R_{cov} can be interpreted as the sum of the covalent radii for Ti and O ions[31] and was determined from the fit to be 2.40 Å. This is slightly larger than the tabulated value of 2.26 Å, which is based on a statistical analysis of several thousand experimentally

DOI: 10.1021/acs.jpclett.8b01067
J. Phys. Chem. Lett. 2018, 9, 2985−2990

obtained crystalline Ti−O bond-lengths.[32] This confirms that crystalline TiO_2 bonds are slightly stronger than the equivalent amorphous bonds. Indeed, the former all lie on the upper part of the Pauling fit in Figure 4. The near overlap of amorphous and crystalline data is an indicator of similar bonding. It shows that fundamental principles of bonding can be obtained from an amorphous model alone, principles that are usually deduced from a limited data set for crystalline phases. The distribution of Ti−O bond-lengths in the amorphous phase reveals the extent of the deformation of the polyhedral building blocks. B-TiO_2 also shows a wide (but smaller) distribution. As a consequence, the distributions of *iterative-Hirshfeld*[33] partial charges in B-TiO_2 and a-TiO_2 are similar (see Supporting Information).

This work contributes to a fundamental understanding of the amorphous state, by showing that it is now, for the first time, possible to quantify the extent of structural similarity between amorphous and crystalline phases, thus shedding light on a controversy debated for more than half a century. The problem was nicely formulated by Gaskell in 1998: "One question more than any other has focused the efforts of those working on the structure of glasses. This is the extent to which the atomic structure can be considered uniform, continuous, with randomness at heart. Alternatively, is the structure essentially inhomogeneous, granular, with some close relationship to the structure of a neighboring crystalline phase?"[34] A definite answer, valid for all amorphous materials, does not exist. Instead, individual systems can show a degree of similarity toward certain crystalline polymorphs, as shown here for the case of TiO_2. The similarity is not necessarily confined to short-range order. For some amorphous systems, the network building units might be very similar to those of a crystalline polymorph, while other systems might show distorted network building units but more intermediate-range order. Consequently, it is difficult to settle the matter solely within a pictorial model. Nonetheless, we show here that the problem can be tackled, for the first time quantitatively, within a rigorous mathematical framework, i.e., by using structural descriptors. The SOAP approach used here can quantify the extent to which additional degrees of topological freedom in a disordered amorphous network can influence the structure, by using crystalline polymorphs as references. It can be readily extended to other systems (e.g., the Si/Ge systems, where the liquid structure is very different from those of the normal crystalline/amorphous phases) to find analogous similarities, to discriminate between amorphous phases of the same material (e.g., prepared in different ways), or even to facilitate the search for structure−property relationships for amorphous materials, e.g., by searching for correlations of a structure-map, as presented in this paper, with properties of interest.

COMPUTATIONAL METHODS

The melt-quench method[35] was used to generate 216-atom amorphous models. For all molecular-dynamics simulations, density functional theory was used with VASP and the PBEsol functional.[36−38] A total simulation time of 130 ps with a 1 fs time step was used to generate the amorphous model in a cubic supercell, with an arbitrary cooling rate of −19.5 K/ps. Since the density of the system is crucial for a correct description of the structure, and the density of bulk amorphous TiO_2 is not known experimentally, special care was devoted to obtaining a good density estimation for the amorphous solid. Time scales needed for the equilibration of the structure with regard to volume changes were much larger than time scales needed for the equilibration with regard to changes in temperature. For this reason, it was not possible to perform the whole quench in the *NpT*-ensemble and to allow for continuous volume equilibration, within 100 ps of cooling time. Instead, starting from a density of 3.21 g cm^{-3} at 2250 K, an experimental volume-temperature relationship for the liquid[39] was followed until a temperature of 1470 K was reached. Below that, the relationship established by Alderman et al. in a classical MD simulation[40] was followed. The *Nosé−Hoover* thermostat,[41−43] as implemented in VASP, was used. Finally, the amorphous model was equilibrated in the *NpH*-ensemble to obtain the density of 3.68 g cm^{-3}. *Parrinello−Rahman* dynamics,[44,45] as implemented in VASP, were used for pressure control. The liquid and amorphous models were validated against experimental data[18,40] by comparing experimental and calculated structure factors. Bond-strengths were calculated using the LOBSTER[46] code.

The average global SOAP kernel, as implemented in the Quippy package[47] was used for the calculation of the SOAP similarity. For a given structure, Gaussian functions are first placed on each of the atoms. The obtained local density of atoms is expanded on a basis composed of a set of orthogonal radial basis functions, $g_b(\mathbf{r})$, and spherical harmonics, $Y_{lm}(\mathbf{r})$.[13,14] The expansion coefficients, c_{blm}, are then averaged over all atoms i, j and the SOAP descriptor for a given structure is given by

$$\overline{p}_{b_1 b_2 l} = \frac{\pi}{N^2}\sqrt{\frac{8}{2l+1}}\sum_m \sum_{i,j} (c^i_{b_1 lm})^\dagger c^j_{b_2 lm} \tag{2}$$

where N is the number of atoms. A measure for the similarity between two structures is given by the dot product of two SOAP descriptors, i.e., the kernel, $\overline{K} = \overline{\mathbf{p}}\cdot\overline{\mathbf{p}}'$. Finally, the structural distance is $\overline{D} = \sqrt{2 - 2\overline{K}}$. The package scikit-learn[48] was used for MDS.

ASSOCIATED CONTENT

Supporting Information

The Supporting Information is available free of charge on the ACS Publications website at DOI: 10.1021/acs.jpclett.8b01067.

Structural parameters (radial-distribution functions, bond-angle distribution functions, dihedral-angle distribution functions, coordination-number distributions, polyhedral connectivity, structure factors, and Hirshfeld-I partial charges) of the generated amorphous and liquid TiO_2 models, together with a detailed description of the methods used (PDF)

AUTHOR INFORMATION

Corresponding Author

*E-mail: sre1@cam.ac.uk.

ORCID

Juraj Mavračić: 0000-0001-5457-4550
Volker L. Deringer: 0000-0001-6873-0278
Stephen R. Elliott: 0000-0002-8202-8482

Notes

The authors declare no competing financial interest.

DOI: 10.1021/acs.jpclett.8b01067
J. Phys. Chem. Lett. 2018, 9, 2985−2990

■ ACKNOWLEDGMENTS

J.M. specially acknowledges the work of Adrian C. Wright. His overview in ref 12 was a great inspiration for this work. J.M. and F.C.M. acknowledge the EPSRC Centre for Doctoral Training in Computational Methods for Materials Science for funding under Grant Number EP/L015552/1. Via our membership of the UK's HEC Materials Chemistry Consortium, which is funded by EPSRC (EP/L000202), this work used the ARCHER UK National Supercomputing Service (http://www.archer.ac.uk). V.L.D. gratefully acknowledges a Feodor Lynen Fellowship from the Alexander von Humboldt Foundation, a Leverhulme Early Career Fellowship, and support from the Isaac Newton Trust.

■ REFERENCES

(1) Senior, J.; Jamro, M. Y. *Optical Fiber Communications: Principles and Practice*, 3rd ed.; Pearson Education Limited: Harlow, England, 2009.

(2) Park, J. S.; Maeng, W. J.; Kim, H. S.; Park, J. S. Review of Recent Developments in Amorphous Oxide Semiconductor Thin-Film Transistor Devices. *Thin Solid Films* **2012**, *520*, 1679−1693.

(3) Goetzberger, A.; Hebling, C.; Schock, H.-W. Photovoltaic Materials, History, Status and Outlook. *Mater. Sci. Eng., R* **2003**, *40*, 1−46.

(4) Wingert, M. C.; Zheng, J.; Kwon, S.; Chen, R. Thermal Transport in Amorphous Materials: A Review. *Semicond. Sci. Technol.* **2016**, *31*, 113003.

(5) Kim, N.; Chae, S.; Ma, J.; Ko, M.; Cho, J. Fast-Charging High-Energy Lithium-Ion Batteries via Implantation of Amorphous Silicon Nanolayer in Edge-Plane Activated Graphite Anodes. *Nat. Commun.* **2017**, *8*, 812.

(6) Lin, L.; Xu, X.; Chu, C.; Majeed, M. K.; Yang, J. Mesoporous Amorphous Silicon: A Simple Synthesis of a High-Rate and Long-Life Anode Material for Lithium-Ion Batteries. *Angew. Chem., Int. Ed.* **2016**, *55*, 14063−14066.

(7) Raoux, S. Phase Change Materials. *Annu. Rev. Mater. Res.* **2009**, *39*, 25−48.

(8) Chen, Q. Z.; Thompson, I. D.; Boccaccini, A. R. 45S5 Bioglass®-Derived Glass-Ceramic Scaffolds for Bone Tissue Engineering. *Biomaterials* **2006**, *27*, 2414−2425.

(9) Hegedus, J.; Elliott, S. R. Computer-Simulation Design of New Phase-Change Memory Materials. Phys. *Phys. Status Solidi A* **2010**, *207*, 510−515.

(10) Loke, D.; Lee, T. H.; Wang, W. J.; Shi, L. P.; Zhao, R.; Yeo, Y. C.; Chong, T. C.; Elliott, S. R. Breaking The Speed Limits of Phase-Change Memory. *Science* **2012**, *336*, 1566−9.

(11) Loke, D.; Skelton, J. M.; Wang, W.-J.; Lee, T.-H.; Zhao, R.; Chong, T.-C.; Elliott, S. R. Ultrafast Phase-Change Logic Device Driven by Melting Processes. *Proc. Natl. Acad. Sci. U. S. A.* **2014**, *111*, 13272−13277.

(12) Wright, A. C. The Great Crystallite Versus Random Network Controversy: A Personal Perspective. *Int. J. Appl. Glass Sci.* **2014**, *5*, 31−56.

(13) Bartók, A. P.; Kondor, R.; Csányi, G. On Representing Chemical Environments. *Phys. Rev. B: Condens. Matter Mater. Phys.* **2013**, *87*, 1−16.

(14) De, S.; Bartók, A. P.; Csányi, G.; Ceriotti, M. Comparing Molecules and Solids Across Structural and Alchemical Space. *Phys. Chem. Chem. Phys.* **2016**, *18*, 13754−13769.

(15) Köhler, T.; Turowski, M.; Ehlers, H.; Landmann, M.; Ristau, D.; Frauenheim, T. Computational Approach for Structure Design and Prediction of Optical Properties in Amorphous TiO_2 Thin-Film Coatings. *J. Phys. D: Appl. Phys.* **2013**, *46*, 325302.

(16) Landmann, M.; Köhler, T.; Köppen, S.; Rauls, E.; Frauenheim, T.; Schmidt, W. Fingerprints of Order and Disorder in the Electronic and Optical Properties of Crystalline and Amorphous TiO_2. *Phys. Rev. B: Condens. Matter Mater. Phys.* **2012**, *86*, 064201.

(17) Prasai, B.; Cai, B.; Underwood, M. K.; Lewis, J. P.; Drabold, D. A. Properties of Amorphous and Crystalline Titanium Dioxide From First Principles. *J. Mater. Sci.* **2012**, *47*, 7515−7521.

(18) Petkov, V.; Holzhüter, G.; Tröge, U.; Gerber, T.; Himmel, B. Atomic-Scale Structure of Amorphous TiO_2 by Electron, X-Ray Diffraction and Reverse Monte Carlo Simulations. *J. Non-Cryst. Solids* **1998**, *231*, 17−30.

(19) Howard, C. J.; Sabine, T. M.; Dickson, F. Structural and Thermal Parameters For Rutile and Anatase. *Acta Crystallogr., Sect. B: Struct. Sci.* **1991**, *47*, 462−468.

(20) Baur, W. H. Atomabstände und Bindungswinkel im Brookit, TiO_2. *Acta Crystallogr.* **1961**, *14*, 214−216.

(21) Ben Yahia, M.; Lemoigno, F.; Beuvier, T.; Filhol, J.; Richard-Plouet, M.; Brohan, L.; Doublet, M. Updated References For the Structural, Electronic, and Vibrational Properties of TiO_2(B) Bulk Using First-Principles Density Functional Theory Calculations. *J. Chem. Phys.* **2009**, *130*, 204501.

(22) Sato, H.; Endo, S.; Sugiyama, M.; Kikegawa, T.; Shimomura, O.; Kusaba, K. Baddeleyite-Type High-Pressure Phase of TiO_2. *Science* **1991**, *251*, 786−788.

(23) Swamy, V.; Dubrovinsky, L. S.; Dubrovinskaia, N. A.; Langenhorst, F.; Simionovici, A. S.; Drakopoulos, M.; Dmitriev, V.; Weber, H. P. Size Effects on the Structure and Phase Transition Behavior of Baddeleyite TiO_2. *Solid State Commun.* **2005**, *134*, 541−546.

(24) Latroche, M.; Brohan, L.; Marchand, R.; Tournoux, M. New Hollandite Oxides: TiO_2(H) and $K_{0.06}TiO_2$. *J. Solid State Chem.* **1989**, *81*, 78−82.

(25) Borg, I.; Groenen, P. J. F. *Modern Multidimensional Scaling: Theory and Applications*; Springer-Verlag: New York, 2005.

(26) Rosenblatt, M. Remarks on Some Nonparametric Estimates of a Density Function. *Ann. Math. Stat.* **1956**, *27*, 832−837.

(27) Parzen, E. On Estimation of a Probability Density Function and Mode. *Ann. Math. Stat.* **1962**, *33*, 1065−1076.

(28) Pauling, L. Atomic Radii and Interatomic Distances in Metals. *J. Am. Chem. Soc.* **1947**, *69*, 542−553.

(29) Dronskowski, R.; Blöchl, P. E. Crystal Orbital Hamilton Populations (COHP): Energy-Resolved Visualization of Chemical Bonding in Solids Based on Density-Functional Calculations. *J. Phys. Chem.* **1993**, *97*, 8617−8624.

(30) Maintz, S.; Deringer, V. L.; Tchougréeff, A. L.; Dronskowski, R. Analytic Projection from Plane-Wave and PAW Wavefunctions and Application to Chemical-Bonding Analysis in Solids. *J. Comput. Chem.* **2013**, *34*, 2557−2567.

(31) Deringer, V. L.; Stoffel, R. P.; Wuttig, M.; Dronskowski, R. Vibrational Properties and Bonding Nature of Sb_2Se_3 and their Implications for Chalcogenide Materials. *Chem. Sci.* **2015**, *6*, 5255−5262.

(32) Cordero, B.; Gómez, V.; Platero-Prats, A. E.; Revés, M.; Echeverría, J.; Cremades, E.; Barragán, F.; Alvarez, S. Covalent Radii Revisited. *Dalton Trans.* **2008**, 2832−2838.

(33) Bultinck, P.; Van Alsenoy, C.; Ayers, P.; Carbó-Dorca, R. Critical Analysis and Extension of the Hirshfeld Atoms in Molecules. *J. Chem. Phys.* **2007**, *126*, 144111.

(34) Gaskell, P. H. The Structure of Simple Glasses: Randomness or Pattern - The Debate Goes On. *Glass Phys. Chem.* **1998**, *24*, 180−188.

(35) Drabold, D. A. Topics in the Theory of Amorphous Materials. *Eur. Phys. J. B* **2009**, *68*, 1−21.

(36) Kresse, G.; Furthmüller, J. Efficient Iterative Schemes for Ab Initio Total-Energy Calculations Using a Plane-Wave Basis Set. *Phys. Rev. B: Condens. Matter Mater. Phys.* **1996**, *54*, 11169−11186.

(37) Kresse, G.; Joubert, D. From Ultrasoft Pseudopotentials to the Projector Augmented-Wave Method. *Phys. Rev. B: Condens. Matter Mater. Phys.* **1999**, *59*, 1758−1775.

(38) Perdew, J.; Ruzsinszky, A.; Csonka, G.; Vydrov, O.; Scuseria, G.; Constantin, L.; Zhou, X.; Burke, K. Restoring the Density-Gradient Expansion for Exchange in Solids and Surfaces. *Phys. Rev. Lett.* **2008**, *100*, 136406.

DOI: 10.1021/acs.jpclett.8b01067
J. Phys. Chem. Lett. 2018, 9, 2985−2990

(39) Dingwell, D. B. The Density of Titanium(IV) Oxide Liquid. *J. Am. Ceram. Soc.* **1991**, *74*, 2718−19.
(40) Alderman, O. L. G.; Skinner, L. B.; Benmore, C. J.; Tamalonis, A.; Weber, J. K. R. Structure of Molten Titanium Dioxide. *Phys. Rev. B: Condens. Matter Mater. Phys.* **2014**, *90*, 094204.
(41) Nosé, S. A. Unified Formulation of the Constant Temperature Molecular Dynamics Methods. *J. Chem. Phys.* **1984**, *81*, 511−519.
(42) Nosé, S. Constant Temperature Molecular Dynamics Methods. *Prog. Theor. Phys. Suppl.* **1991**, *103*, 1−46.
(43) Hoover, W. G. Canonical Dynamics: Equilibrium Phase-Space Distributions. *Phys. Rev. A: At., Mol., Opt. Phys.* **1985**, *31*, 1695−1697.
(44) Parrinello, M.; Rahman, A. Crystal Structure and Pair Potentials: A Molecular Dynamics Study. *Phys. Rev. Lett.* **1980**, *45*, 1196−1199.
(45) Parrinello, M.; Rahman, A. Polymorphic Transitions in Single Crystals: A New Molecular Dynamics Method. *J. Appl. Phys.* **1981**, *52*, 7182−7190.
(46) Maintz, S.; Deringer, V. L.; Tchougréeff, A. L.; Dronskowski, R. LOBSTER: A Tool to Extract Chemical Bonding from Plane-Wave Based DFT. *J. Comput. Chem.* **2016**, *37*, 1030−1035.
(47) Bartók, A. P.; Csányi, G. Gaussian Approximation Potentials: A Brief Tutorial Introduction. *Int. J. Quantum Chem.* **2015**, *115*, 1051−1057.
(48) Pedregosa, F.; Varoquaux, G.; Gramfort, A.; Michel, V.; Thirion, B.; Grisel, O.; Blondel, M.; Prettenhofer, P.; Weiss, R.; Dubourg, V.; et al. Scikit-learn: Machine Learning in Python. *J. Mach. Learn. Res.* **2011**, *12*, 2825−2830.

DOI: 10.1021/acs.jpclett.8b01067
J. Phys. Chem. Lett. 2018, 9, 2985−2990